

# Aggregation of chemotactic organisms in an advected environment

Javier Muñoz-García<sup>1,2</sup> and Zoltán Neufeld<sup>1</sup>

<sup>1</sup> School of Mathematical Sciences and Complex and Adaptive Systems Laboratory, University College Dublin, Belfield, Dublin 4, Ireland

<sup>2</sup> Grupo Interdisciplinar de Sistemas Complejos (GISC)

E-mail: javiermunozgarcia@gmail.com

**Abstract.** We study the effect of advection on the aggregation and pattern formation in chemotactic systems described by Keller-Segel type models. The evolution of small perturbations is studied analytically in the linear regime complemented by numerical simulations. We show that an uniform flow can significantly alter the spatial structure and dynamics of the chemotactic system. The flow leads to the formation of anisotropic aggregates that move following the direction of the flow, although the chemotactic cells are not directly advected by the flow. Sufficiently strong advection stops the aggregation and suppresses the coarsening process that is thus restricted to the direction perpendicular to the flow.

PACS numbers: 87.18.Ed 87.18.Hf 82.39.Rt 47.63.-b 47.20.-k

## 1. Introduction and model

Directed motion of microorganisms and cells in response to chemical signals - *chemotaxis* - plays an important role in a wide range of biological processes including migration of white blood cells, cancer invasion [1], embryonic development or in locating nutrients by bacteria, algae etc [2, 3]. In many cases the chemotactic cells not only detect, but also produce chemical signals that may attract other members of the population. This type of communication based on chemoattractant odors or pheromones can control group behavior, aggregation, swarming and collective decisions (quorum sensing) in bacterial colonies [4], slime mold [5] or insect populations. Often the medium into which the chemical signal is released is not stationary but is a moving fluid (e.g. air or water) while the chemotactic cells or organisms are not transported by the flow as they are bound to a solid surface (e.g. microbial biofilm communities in natural environments or bioreactors). In the case of non-linear chemical reactions Rovinsky and Menzinger has shown that such differential flow can induce a pattern forming instability in systems involving activator and inhibitor kinetics [6, 7]. In this Letter we consider the effects of differential advection by a uniform flow on the aggregation and pattern formation in chemotactic biological populations.

A well known classical continuum model of chemotaxis at the population level is the Keller-Segel (KS) model [5], that describes the evolution of the density of chemotactic cells,  $u(\mathbf{x}, t)$ , and the chemoattractant concentration,  $v(\mathbf{x}, t)$ . When the chemical field  $v$  is advected by a uniform flow  $\mathbf{V}$  and the density field evolves on a fixed substrate we have

$$\frac{\partial u}{\partial t} = \nabla \cdot (D_u \nabla u - \chi(u) \nabla v), \quad (1)$$

$$\frac{\partial v}{\partial t} = D_v \nabla^2 v + fu - sv - \mathbf{V} \cdot \nabla v. \quad (2)$$

$D_u$  and  $D_v$  are constant diffusivities and the chemoattractant is assumed to be produced proportionally to the local cell density and has a constant degradation rate,  $s$ . Assuming no-flux or periodic boundary conditions the total mass of the biological component is conserved and can be characterized by the average density. In the original KS model [5, 8]  $\mathbf{V} = 0$  and the chemotactic flux is proportional to the particle density, i.e.  $\chi(u) = \chi_0 u$ . Extensions of this model with more general forms for  $\chi(u)$  have also been studied such as the chemotaxis model with prevention of overcrowding introduced in Ref. [9] where  $\chi(u) = \chi_0 u(1 - u/\gamma)$ . An important feature of the KS model (observed in biological systems such as slime mold populations) is that it demonstrates an aggregation instability when the total mass of cells is larger than a certain threshold. Properties of the solutions of the KS system and its variants have been studied extensively (for recent reviews see Refs. [10] and [11]). Interesting analogies between KS type chemotaxis models and nonlinear mean field Fokker-Planck equations and generalized thermodynamics have been pointed out in [12].

## 2. Linear Analysis

First we consider the stability of the spatially uniform solution. Assuming a uniform initial condition  $u(t=0) \equiv u_0$  and  $v(t=0) \equiv v_0$  all spatial derivatives vanish in Eqs. (1) and (2) and we have the solutions  $u(t) = u_0$  and  $v(t) = fu_0/s + (v_0 - fu_0/s)e^{-st}$ . Thus, independently of the initial conditions the concentration tends to a constant value  $fu_0/s$  for large times. To investigate pattern forming instability in this system we consider the evolution of spatially non-uniform periodic perturbations added to the uniform steady state of the form  $u(\mathbf{x}, t) = u_0 + \hat{u} \exp[i\mathbf{q} \cdot \mathbf{x} + \omega(\mathbf{q})t]$  and  $v(\mathbf{x}, t) = fu_0/s + \hat{v} \exp[i\mathbf{q} \cdot \mathbf{x} + \omega(\mathbf{q})t]$ , and study whether the perturbation is amplified or damped out in the course of time. Here  $\mathbf{q}$  is the wave vector of the perturbation,  $\omega(\mathbf{q})$  is the corresponding dispersion relation, and  $\hat{u}$  and  $\hat{v}$  are the amplitudes of the perturbation at  $t=0$ . Substituting these expressions into (1) and (2), and neglecting quadratic terms in  $\hat{u}$ ,  $\hat{v}$ , we obtain a linear system of equations where non-trivial solutions only exist if the determinant of the coefficient matrix is equal to zero. In contrast to previous chemotactic models where advection is not considered, the resulting quadratic equation for the dispersion relation has complex coefficients and reads

$$\omega^2 + \omega(a + ib) + (c + id) = 0. \quad (3)$$

The coefficients  $a$ ,  $b$ ,  $c$ , and  $d$  are functions of parameters and wave-vector components yielding

$$a = (D_v + D_u)q^2 + s \quad (4)$$

$$b = \mathbf{V} \cdot \mathbf{q} \quad (5)$$

$$c = D_v D_u q^4 + [s D_u - f\chi(u_0)] q^2 \quad (6)$$

$$d = D_u q^2 \mathbf{V} \cdot \mathbf{q}. \quad (7)$$

The real and imaginary parts corresponding to the two complex solutions are‡

$$\text{Re}(\omega^\pm) = -\frac{a}{2} \pm \frac{1}{2\sqrt{2}} \{ [(a^2 - b^2 - 4c)^2 + (2ab - 4d)^2]^{1/2} + a^2 - b^2 - 4c \}^{1/2}, \quad (8)$$

$$\text{Im}(\omega^\pm) = -\frac{b}{2} \pm \frac{\text{sgn}(2ab - 4d)}{2\sqrt{2}} \{ [(a^2 - b^2 - 4c)^2 + (2ab - 4d)^2]^{1/2} - a^2 + b^2 + 4c \}^{1/2}, \quad (9)$$

The real part of  $\omega$  gives the growth or decay rate of the perturbation amplitude. In particular, the mode corresponding to the maximum of  $\text{Re}(\omega)$ , which we denote by  $\mathbf{q}^l$ , determines the characteristic wavelength of the pattern in the linear regime, while the imaginary part describes its propagation in space. The velocity  $\mathbf{V}^l$  at which the instability travels across the substrate, corresponding to the *phase velocity* of the mode  $\mathbf{q}^l$ , satisfies the relationship [14]

$$\mathbf{V}^l \cdot \mathbf{q}^l = -\text{Im} [\omega(\mathbf{q}^l)]. \quad (10)$$

The negative branch of the dispersion relation is unconditionally stable, i.e.  $\text{Re}(\omega^-) < 0$ , but the positive branch may produce non-trivial dynamics and pattern

‡ See for example page 95 of Mostowski and Stark [13]

formation for a certain range of wavenumbers. Some insight into the behavior of the system can be obtained by investigating the limiting cases of small and large wavelengths. For large values of  $q$  we can expand Eq. (8) to obtain  $\text{Re}(\omega^+) = -D_u q^2$ , therefore the amplitude of perturbations decays exponentially for these modes. In the case of large wavelength perturbations the expansion to the lowest orders in  $q$  yields

$$\begin{aligned} \text{Re}(\omega^+) = & \left[ \frac{f\chi(u_0)}{s} - D_u \right] q^2 \\ & - \frac{f\chi(u_0)}{s^3} q^2 \{ [(D_v - D_u)s + f\chi(u_0)]q^2 + (\mathbf{V} \cdot \mathbf{q})^2 \} + \mathcal{O}(q^6). \end{aligned} \quad (11)$$

Thus, when  $fs^{-1}\chi(u_0) - D_u > 0$  the positive branch has a band of unstable modes for small wave vectors. In the case of the standard KS model,  $\chi(u_0) = \chi_0 u_0$ , the above condition is equivalent to the aggregation threshold:  $u_0 > D_u s (f\chi_0)^{-1}$  [5, 8]. In Eq. (11) we observe that the advection velocity appears at the order  $q^4$ . This means that, when the above condition for instability is satisfied, there is always a band of unstable modes with long wavelengths around  $q = 0$ , but the range of unstable modes and their growth rate decreases with the advection velocity. This stabilizing effect of the flow is in contrast with the behavior of reaction-diffusion systems studied by Rovinsky and Menzinger [6, 7] where the differential flow induces an instability at a finite wavelength. For the imaginary part of  $\omega$ , we have the following expansion of Eq. (9) for small wave vectors:

$$\text{Im}(\omega^+) = -fs^{-2}\chi(u_0)q^2 (\mathbf{V} \cdot \mathbf{q}) + \mathcal{O}(q^5). \quad (12)$$

Therefore, although the particle density is not directly advected by the flow, using Eq. (10) we see that the chemotaxis induces a phase velocity,  $\mathbf{V}^l$ , that is inversely proportional to the square of the wavelength and, consequently, it is small relative to the advection velocity.

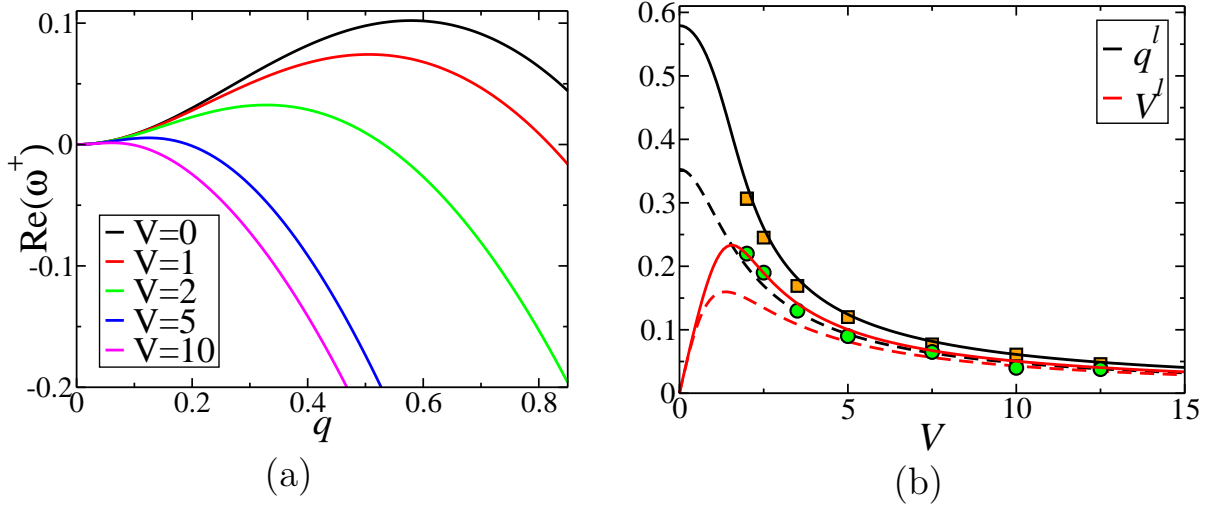
### 3. Pattern formation in one dimension

Figure 1(a) shows the effect of the advection velocity on the real part of the dispersion relation given by Eq. (8) for a 1D system. When  $V$  increases the wavenumber of the dominant mode corresponding to the maximum of  $\text{Re}(\omega^+)$ ,  $q^l$ , decreases [Fig. 1(b)]. In fact, from the expansion of Eq. (8) for small  $q$  given by Eq. (11) we have  $q^l = [\nu / (2\mathcal{K})]^{1/2}$  with  $\nu = f\chi(u_0)s^{-1} - D_u$  and  $\mathcal{K} = f\chi(u_0)s^{-3} [(D_v - D_u)s + f\chi(u_0) + V^2]$ . Thus for large  $V$ , the dominant wavelength in the linear regime,  $\lambda^l = 2\pi/q^l$ , is proportional to the advection velocity. The phase velocity of the spatial pattern [Eq. (10)] is also shown in Fig. 1(b) as a function of the advection velocity for the exact dispersion relation [Eq. (9)]. We notice that the phase velocity has a maximum for a certain value of  $V$ . Thus, surprisingly, when the advection velocity is increased beyond this value, the phase velocity of the pattern decreases as  $V$  is increased. This non-monotonic dependence can also be shown using the expansion of  $\text{Im}(\omega^+)$  for small wavenumber modes [Eq. (12)]

from where a compact analytical expression for the phase velocity is obtained [see Fig. 1(b)]

$$V^l = \frac{f\chi(u_0)}{s^2} (q^l)^2 V = \frac{[f\chi(u_0) - D_u s] V}{2[(D_v - D_u) s + f\chi(u_0) + V^2]}. \quad (13)$$

Although this expression is only valid for small values of  $q^l$ , it is qualitatively similar to the exact solution and already shows that when  $V$  exceeds an certain threshold,  $V_t = \sqrt{(D_v - D_u) s + f\chi(u_p)}$ , stronger advection induces slower pattern movement.



**Figure 1.** (a) Real part of the dispersion relation  $\text{Re}(\omega^+)$  given by Eq. (8) as a function of  $q$  for a 1D system with  $D_u = D_v = f = s = \gamma = 1$ ,  $\chi(u_0) = 10u_0(1 - u_0/\gamma)$ , and  $u_0 = 0.25$ , for different values of the advection velocity,  $V$ . (b)  $q^l$  (black lines) and  $V^l$  (red lines) as a function of the advection velocity. The solid lines represent the exact solution obtained from (8) and (9). The dashed lines represent the approximate solution for small wavelengths. The velocity of the pattern and the dominant mode measured from the numerical simulations are represented by circles and squares respectively.

For the numerical simulations we use the chemotactic response function:  $\chi(u) = \chi_0 u(1 - u/\gamma)$ , that avoids the singularities associated with other models. Interestingly, we have also found that in the case of the standard linear response,  $\chi(u) = \chi_0 u$ , advection can suppress the singularity and produce qualitatively similar behavior to the previous function when  $V$  is sufficiently large. We consider periodic boundary conditions with initial fields in the uniform steady state with a small amplitude random perturbation.

Representative 1D numerical simulations for the evolution of the density profile,  $u(x, t)$  are shown in Fig. 2 for two  $V$  values of the advection velocity. In the case of  $V = 1$  [Fig. 2(a)] we observe a slow coarsening process which tends to reduce the number of structures as observed in the system without advection [9]. However, for  $V = 5$  [Fig. 2(b)] after a short transient a periodic pattern with constant wavelength develops. As shown in Fig. 2, in the presence of advection the  $x \rightarrow -x$  symmetry of the profiles is broken [see also Fig. 3(a)] and the pattern propagates in the positive direction (i.e. in

the direction of the advection velocity). In the absence of coarsening (i.e. for values of  $V \gtrsim 2$ ) the pattern moves uniformly with a well defined velocity as shown in Fig. 2(b). The velocity of the pattern was measured for different values of  $V$  and is plotted in Fig. 1(b). The measured velocity agrees well with the analytical results obtained from the linear stability analysis. The behavior of the chemoattractant concentration,  $v$ , is very similar to the density profiles, as shown in Fig. 3(a) where the profiles of  $u$  and  $v(s/f)$  are plotted together for different values of  $V$ . Figure 3(b) shows the temporal evolution of the wavelength  $\lambda(t)$  (measured as two times the average distance between consecutive minima and maxima) for different values of  $V$ . When the advection is strong enough there is no coarsening, the wavelength becomes constant and, as predicted by the linear analysis, its value is proportional to  $V$  [Fig. 1(b)]. Thus the nonlinear effects (such as coarsening) are avoided for large values of  $V$  and the system remains in the linear regime. Similar results are obtained for the standard KS model, with the difference that for slow advection the numerical simulations do not reach a stationary state, indicating an aggregation singularity with unlimited growth of the density in some points.

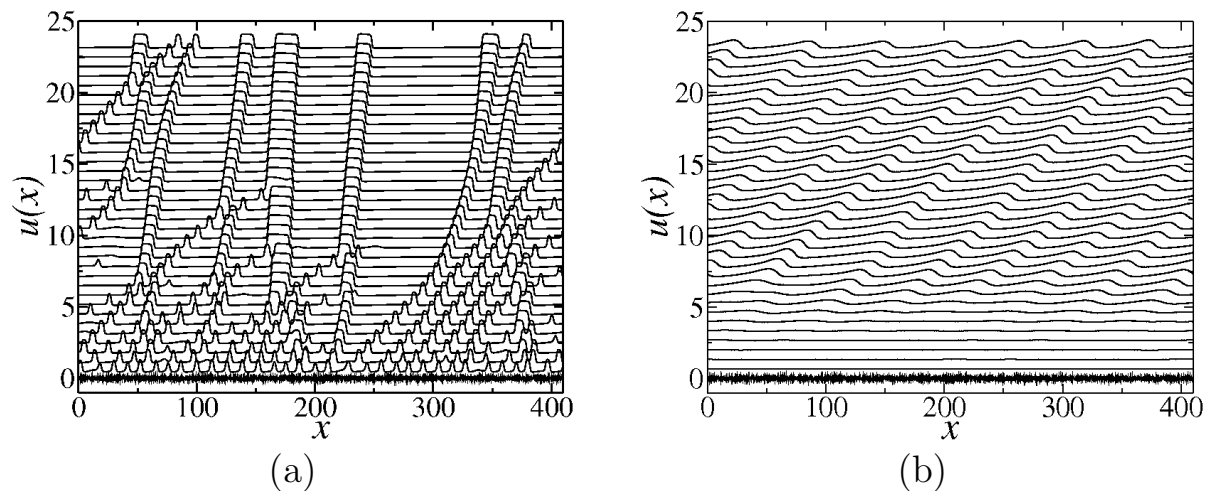


**Figure 2.** (a) Density profiles at equally spaced times (profiles are offset vertically) between  $t = 0$  (bottom) and  $t = 3500$  (top) for: (a)  $V = 1$  and (b)  $V = 5$ .

#### 4. Pattern formation in two dimensions

The effect of the advection term in the real part of the dispersion relation given by Eq. (8) for a  $2D$  system is shown in Fig. 4. Without loss of generality we assume that the advection is along the  $x$ -axis. Thus, we can write  $\mathbf{V} = (V, 0)$  and we plot  $\text{Re}(\omega^+)$  as a function of  $q_x$  and  $q_y$  for different values of  $V$ . When  $V = 0$  the system is isotropic and all the wavevectors within a distance  $q^l$  from the origin maximize  $\text{Re}(\omega^+)$  [Fig. 4(a)]. When  $V$  is nonzero, the maximum is oriented along the  $y$ -axis but the absolute value is not affected by the value of  $V$  [Fig. 4(b)]. The effect of the advection on the wavelength and orientation of the pattern can be analyzed in the small  $q$  limit using

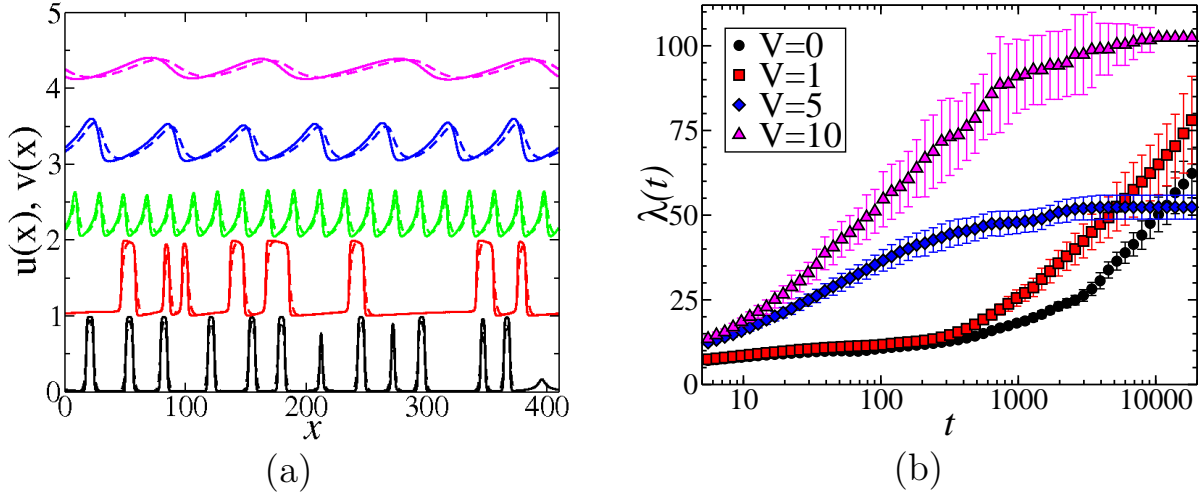


**Figure 3.** (a) Density,  $u$ , (solid line) and signal concentration,  $v$ , (dashed line) profiles at  $t = 3500$  for  $V = 0, 1, 2, 5$ , and  $10$ , from bottom to top respectively (profiles are offset vertically). (b) Temporal evolution of the lateral pattern wavelength,  $\lambda(t)$ , for different values of  $V$ . Error bars represent the standard deviation calculated from 150 different random initial conditions.

Eq. (11). It can be shown that the dominant mode is always oriented along the  $y$ -axis and its value is  $q_y^l = [\nu / (2\mathcal{K}_y)]^{1/2}$  where  $\mathcal{K}_y = f\chi(u_0)s^{-3}[(D_v - D_u)s + f\chi(u_0)]$  and  $\nu$  is the same as defined for the 1D case (see Appendix). Thus, in contrast to the one-dimensional system, the observed dominant wavelength of the pattern in the linear regime is independent of the advection velocity  $V$ , although the features of the pattern are altered by the symmetry breaking induced by the advection. For the phase velocity, using the expansion of  $\text{Im}(\omega^+)$  for small  $q$  and Eq. (10) we have  $\mathbf{V}^l \cdot \mathbf{q}^l / q^l = f\chi(u_p)s^{-2}q^l(\mathbf{V} \cdot \mathbf{q}^l) = 0$  because  $\mathbf{V} = (V, 0)$  and  $\mathbf{q}^l = (0, q_y^l)$ . Therefore, the dominant mode in the pattern is not moving since it is oriented in the  $y$  axis that is perpendicular to the advection velocity. However, for modes in the  $x$ -axis,  $q_x$ , the phase velocity in this direction is  $V_x^l = f\chi(u_0)s^{-2}q_x^2V$  which is proportional to the advection velocity and increases with the wavenumber.

Two-dimensional numerical simulations were performed using a cubic interpolation semi-lagrangian scheme [15] for the advection. For the spatial discretization of the particle density we used the method proposed recently by Grima and Newman [16], that allows for an accurate analysis of the evolution of the system without the dissipative effects of other schemes. In the absence of advection a slow coarsening process occurs in which, after long times, the cells accumulate into a single aggregate [9]. When advection takes place the resulting pattern is not isotropic and the dominant wave vector is oriented along the  $y$  axis. The temporal evolution of  $u$  for different values of the advection velocity is shown in Fig. 5 [as in the 1D case, the evolution of the chemical field is very similar to the density field (see supplementary material)]. As predicted above, the pattern does not propagate in the  $y$  direction and the coarsening process along the  $y$  axis is not affected by the advection (see supplementary movies). Thus, in this direction the pattern features

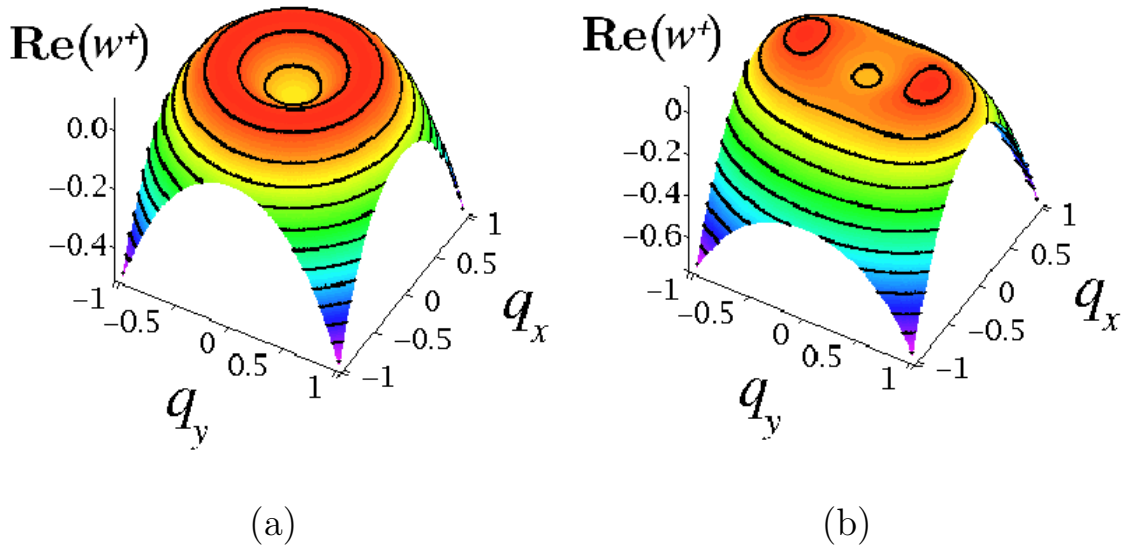


**Figure 4.** Real part of the dispersion relation  $\text{Re}(\omega^+)$  given by Eq. (8) as a function of  $q_x$  and  $q_y$  for a 2D system with (a)  $V = 0$  and (b)  $V = 2$ .

remain the same when the advection velocity is increased. A different scenario is found in the  $x$  direction where the pattern moves with a velocity which increases with  $V$ . The simulations also show that smaller aggregates move faster than larger ones, consistently with the dependence of the phase velocity on the wave-number in the linear analysis. As in the 1D case, the characteristic wavelength of the pattern in the  $x$  direction increases with  $V$ . For slow advection there is a clear coarsening which leads to smaller propagation velocity of the aggregate as predicted above. For finite system sizes and large values of the advection velocity, the wavelength of the dominant linear instability in the  $x$  direction becomes larger than the system size and the resulting pattern is homogeneous in the  $x$  direction, resulting in a static pattern in this direction (see Fig. 5 for  $V = 10$ ).

## 5. Conclusions

We have shown that the inclusion of advection represents a new scenario in Keller-Segel type models with important consequences for the system dynamics and the aggregation of organisms. Here we have presented analytical and computational results on the effect of advective fluid transport and found that the resulting pattern moves following the direction of the flow, although the chemotactic cells are not directly advected. In general, the differential advection has a stabilizing effect which can suppress the coarsening and stop the chemotactic aggregation process. We have analytically derived and checked numerically that in the 1D case larger flows may induce slower aggregation movement. For 2D system the advection of the chemoattractant field by an uniform flow transforms the aggregating spots into an anisotropic pattern of elongated stripes and, although an

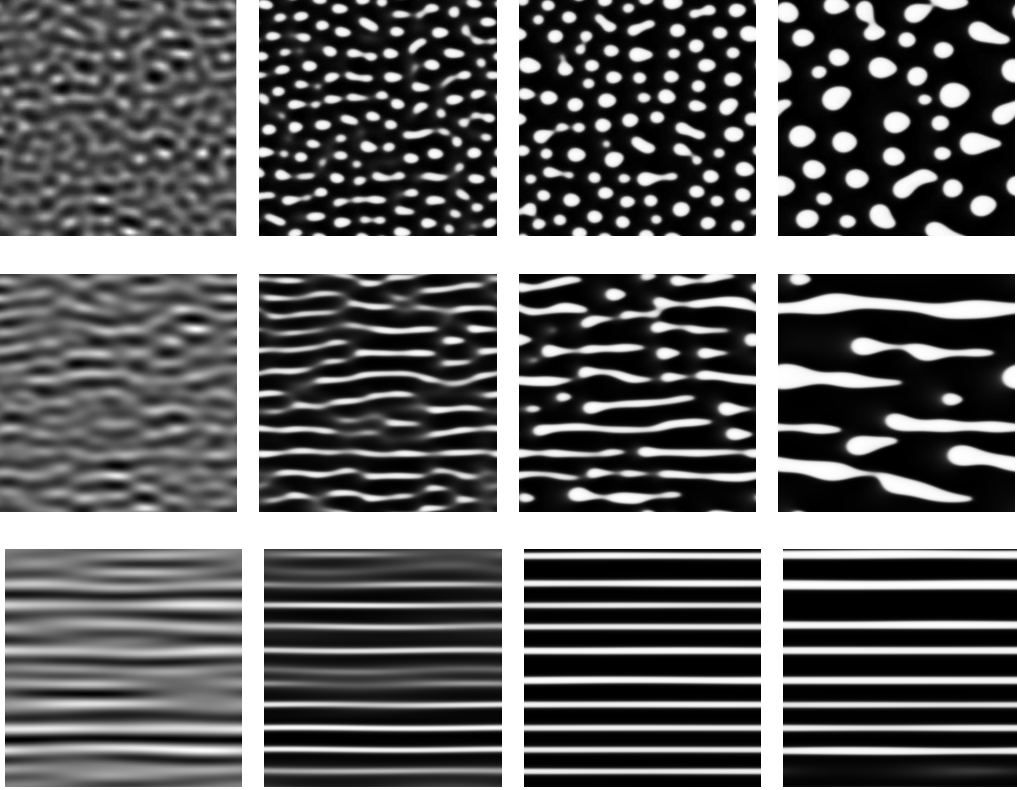


**Figure 5.** Temporal evolution of  $u$  for different values of  $V$ :  $V = 1$  (first row),  $V = 2$  (second row),  $V = 10$  (third row); and different times:  $t = 35$  (first column),  $t = 70$  (second column),  $t = 200$  (third column),  $t = 870$  (fourth column). The  $x$  axis is horizontally oriented. See also supplementary movies.

uni-directional flow does not suppress the coarsening in the perpendicular direction. We expect that more general two-dimensional or time-dependent velocity fields may stop the aggregation completely. It would be interesting to test these predictions experimentally and use this work as a starting point for more general studies of biological pattern formation in advected environments.

### Acknowledgments

This work has been supported by Science Foundation Ireland RFP research grant. Computational facilities were provided by ICHEC.

### Appendix

The experimentally observed pattern is mainly oriented along the direction which yields the maximum value of the real part of the dispersion relation and its wavelength is associated to the wave vector  $\mathbf{q}^l = (q_x^l, q_y^l)$ . This vector verifies

$$\left[ \frac{\partial \text{Re}(\omega^+)}{\partial q_x} \right]_{\mathbf{q}^l} = \left[ \frac{\partial \text{Re}(\omega^+)}{\partial q_y} \right]_{\mathbf{q}^l} = 0, \quad (\text{A.1})$$

which have the following real independent solutions

$$\mathbf{q}_0 = (0, 0), \quad \mathbf{q}_1 = \left( \sqrt{\frac{\nu}{2\mathcal{K}}}, 0 \right), \quad \mathbf{q}_2 = \left( 0, \sqrt{\frac{\nu}{2\mathcal{K}_y}} \right), \quad (\text{A.2})$$

where  $\nu$ ,  $\mathcal{K}$ , and  $\mathcal{K}_y$  are defined as in the main text and assumed positive. In order to decide which of the remaining solutions provide the absolute maximum of  $\text{Re}(\omega^+)$ , we finally substitute the wave vectors given by (A.2) into Eq. (11); we obtain simply

$$[\text{Re}(\omega^+)]_{\mathbf{q}_0} = 0, \quad [\text{Re}(\omega^+)]_{\mathbf{q}_1} = \frac{\nu^2}{4\mathcal{K}}, \quad [\text{Re}(\omega^+)]_{\mathbf{q}_2} = \frac{\nu^2}{4\mathcal{K}_y}, \quad (\text{A.3})$$

from where, since  $\mathcal{K} > \mathcal{K}_y$  for  $V \neq 0$ , we conclude that  $\mathbf{q}^l = \mathbf{q}_2$ .

## References

- [1] A.R.A. Anderson and M.A.J. Chaplain. Continuous and discrete mathematical models of tumor-induced angiogenesis. *Bull. Math. Biol.*, 60:857, 1998.
- [2] Howard C. Berg. Motile behavior of bacteria. *Physics Today*, 1:24, 2000.
- [3] N. Blackburn, T. Fenchel, and J. Mitchell. Microscale nutrient patches in planktonic habitats shown by chemotactic bacteria. *Science*, 282:2254, 1998.
- [4] E.O. Budrene and H.C. Berg. Complex patterns formed by motile cells of escherichia coli. *Nature*, 349:630, 1991.
- [5] E. F. Keller and L. A. Segel. Initiation of slime mold aggregation viewed as an instability. *J. Theor. Biol.*, 26:399, 1970.
- [6] Arkady B. Rovinsky and Michael Menzinger. Chemical instability induced by a differential flow. *Phys. Rev. Lett.*, 69:1193, 1992.
- [7] Arkady B. Rovinsky and Michael Menzinger. Differential flow instability in dynamical systems without an unstable (activator) subsystem. *Phys. Rev. Lett.*, 72:2017, 1994.
- [8] Vidyanand Nanjundiah. Chemotaxis signal relaying and aggregation morphology. *J. Theor. Biol.*, 42:63, 1973.
- [9] Thomas Hillen and Kevin Painter. Global existence for a parabolic chemotaxis model with prevention of overcrowding. *Adv. Appl. Math.*, 26:280, 2001.
- [10] D. Horstmann. From 1970 until present: the keller segel model in chemotaxis and its consequences, Part I. *Jahresbericht der DMV*, 105:103, 2003.
- [11] T. Hillen and K. Painter. A user's guide to pde models for chemotaxis. *J. Math. Biol.*, 58:183, 2009.
- [12] PH Chavanis. Nonlinear mean field fokker-planck equations. application to the chemotaxis of biological populations. *Eur. Phys. J. B*, 62:179, 2008.
- [13] A. Mostowski and M. Stark. *Introduction to Higher Algebra*. Pergamon Press, Oxford, 1964.
- [14] R. M. M. Mattheij, S. W. Rienstra, and J. H. M. Ten Thije Boonkamp. *Partial Differential Equations: Modeling, Analysis, Computation*. Society for Industrial and Applied Mathematics, Philadelphia, PA, USA, 2005.
- [15] Dale R. Durran. *Numerical Methods for wave equations in geophysical and fluid dynamics*. Springer-Verlag New York, New York, 1999.
- [16] R. Grima and T. J. Newman. Accurate discretization of advection-diffusion equations. *Phys. Rev. E*, 70:036703, 2004.